arXiv:1304.6596v1 [physics.optics] 24 Apr 2013

Graphene–Based Optical Phase Modulation

Michele Midrio,[1] **Paola Galli,**[1] **Marco Romagnoli,**[2,*]
Lionel C. Kimerling,[3] **Jurgen Michel**[3]

[1] *Dipartimento di Ingegneria Elettrica Gestionale e Meccanica,*
Università degli Studi di Udine, 33100 Udine, Italy.
[2] *CNIT National Laboratory of Photonic Networks, 56124 Pisa, Italy.*
[3] *Massachusetts Institute of Technology, 77 Massachusetts Ave., Cambridge, MA 02139, USA.*

**marco.romagnoli@cnit.it*

Abstract: In this paper we report phase modulation obtained by inducing a capacitive charge on graphene layers embedded in the core of a waveguide. There is a biasing regime in which graphene absorption is negligible but large index variations can be achieved with a voltage-length product as small as $V_\pi L_\pi \simeq 0.04\,\mathrm{V\,cm}$. Examples of phase induced changes are computed for straight waveguides and for microring resonators showing the possibility to implement several optoelectronic functionalities as modulators, tunable filters, and switches.

© 2013 Optical Society of America

OCIS codes: (250.4110) Modulators; (250.3140) Integrated optoelectronic circuits; (160.3130) Integrated optics materials; (060.4510) Optical communications

---

References and links

1. A. K. Geim, and K. S. Novoselov, "The rise of graphene," Nature Materials **6**, 183–191 (2007).
2. G. T. Reed, *Silicon Photonics*, (John Wiley & Sons, Chichester, England, 2008).
3. J. Liu, M. Beals, A. Pomerene, S. Bernardis, R. Sun, J. Cheng, L. C. Kimerling, and J. Michels, "Waveguide–integrated, ultralow–energy GeSi electro–absorption modulators," Nature Photonics, **2**, 433–437 (2008).
4. G. T. Reed, G. Mashanovich, F. Y. Gardes and D. J. Thomson, "Silicon optical modulators," Nature Photonics, **4**, 518526 (2010)
5. M. Liu, X. Yin, E. Ulin-Avila, B. Geng, T. Zentgraf, L. Ju, F. Wang and X. Zhang. "A graphene-based broadband optical modulator," Nature, **474**, 64 -67 (2011).
6. M. Liu, X. Yin, and X. Zhang, "Double–Layer Graphene Optical Modulator," Nano Lett., **12**, 1482–1485 (2012).
7. S. J. Koester, and M. Li, "High–speed waveguide–coupled graphene–on–graphene optical modulators," Appl. Phys. Lett, **100**, 171107 (2012).
8. M. Midrio, S. Boscolo, M. Moresco, M. Romagnoli, C. De Angelis, A. Locatelli, and A.D. Capobianco, "Graphene-assisted critically-coupled optical ring modulator," Opt. Expr., **20**, 23144-23155 (2012).
9. T. Stauber, N. M. R. Peres, and A. K. Geim, "Optical conductivity of graphene in the visible region of the spectrum," Phys. Rev. B, **78**, 085432 (2008).
10. G. W. Hanson, "Dyadic Green's function and guided surface waves for a surface conductivity model of graphene," J. Appl. Phys., **103**, 064302 (2008).
11. A. Yariv, "Critical Coupling and Its Control in Optical Waveguide–Ring Resonator Systems," IEEE Photon. Technol. Lett., **14**, 483–485 (2002).

---

1. Introduction

Fundamental properties and potential applications of carbon-based structures are of interest in emerging nanoelectronics and nanophotonics. Graphene is a planar atomic layer of carbon atoms bonded in a hexagonal structure that has shown fundamental physical properties different from those of semiconductors [1]. In graphene, the energy-momentum dispersion is linear over a wide range of energies in contrast to the typical parabolic shape of semiconductor valence and conduction bands. This linearity leads to a zero gap and to a massless condition for electrons with a consequent energy independent velocity analogous to sound waves. Another property of graphene is the single layer, or 2D, structure that leads to an enhancement of the interface electric field that may be used for controlling large carrier concentrations with low gating voltages. Integrated optical modulators in silicon are key components in an photonic circuit. The basic mechanisms that alters the amplitude or phase of the propagating light are based on different effects. Plasma dispersion effect is the most used, in this case electrically induced change in the carrier concentration provides a change in material absorption and refractive index proportional to the carrier density [2]. However due to the nature of the physical mechanism phase or amplitude variation never act independently. In addition, residual carrier density occurring under modulation or partial field overlap with electrodes limitate performances in extinction ratio or in insertion loss. Franz Keldish or Quantum Confined Stark effect (QCSE) are alternative mechanisms used in Ge pin or in Ge and III-V quantum wells [3, 4]. In these cases the effect is limited to the spectral band near the semiconductor band edge. As for plasma dispersion based devices even in this case insertion loss due to carriers must be traded off at the expenses of a large extinction ratio.

Recently a single sheet of graphene on a silicon waveguide has been reported to provide an efficient low consumption electro absorption modulation [5]. In the reported modulator the interband transitions of photo-generated electrons are modulated over broad spectral ranges by the drive voltage, so an efficient broadband optical graphene modulator has been demonstrated.

In the present paper we will show that in a certain range of biasing voltages it is possible to discriminate amplitude modulation against phase modulation. This property is specific of graphene and indicates that beyond the conventional amplitude modulation already demonstrated in ref.[5], graphene can be used as a phase modulator with negligible contribution in amplitude modulation and insertion loss.

The wavelength independence of graphene along with the unique property of bias induced separation of electroabsorption and electro refractive index modulation makes this material suitable for highly efficient and broadband modulator for complex modulation formats. The very low insertion loss is also fundamental for the power budget of the link. In this paper we will examine the modulator performances for either a straight waveguide and for a ring based all pass geometry with the aim to envisage the best operating conditions for implementing an efficient and highly performing modulator for complex phase and amplitude modulation formats. We will also highlight that biasing a graphene multilayer requires parallel bias rather than in series as already shown for multilayer graphene electro-absorption modulators [6, 7, 8].

2. Principle of operation

One of the many remarkable and unique properties of graphene is that its complex conductivity can be tuned, even at optical frequencies, by varying the applied chemical potential, i.e. by adding or removing charges from the graphene sheet.

Stauber and co-authors have derived the following expressions for the dependence of the real and imaginary graphene's conductivity on frequency (ω), temperature (T) and applied chemical potential (μ_C) [9]:

$$\sigma_{\mathrm{R}} = \frac{\sigma_0}{2}\left[1+\left(\frac{\hbar\omega}{6q}\right)^2\right]\left(\tanh\frac{\hbar\omega+2\mu_C}{4k_BT}+\tanh\frac{\hbar\omega-2\mu_C}{4k_BT}\right) \quad , \tag{1}$$

$$\sigma_{\mathrm{I}} = \frac{4\sigma_0}{\pi\hbar\omega}\left(\mu_C - \frac{2\mu_C^3}{9q^2}\right) - \frac{\sigma_0}{\pi}\left[1+\left(\frac{\hbar\omega}{6q}\right)^2\right]\log\left|\frac{\hbar\omega+2\mu_C}{\hbar\omega-2\mu_C}\right| \quad , \tag{2}$$

where $q = 2.7\,\mathrm{eV}$ is the hopping parameter, $\hbar$ and k_B are the reduced Planck's and Boltzmann constants, respectively, and

$$\sigma_0 = \frac{e^2}{4\hbar} \simeq 6.0853\times 10^{-5}\,\mathrm{Siemens} \quad , \tag{3}$$

with e the electron charge. The relative dielectric constant of graphene is simply related to the imaginary part of its conductivity as follows:

$$\varepsilon_r = 1 - \frac{\sigma_{\mathrm{I}}}{\omega\varepsilon_0} \quad , \tag{4}$$

with $\varepsilon_0 = 8.85\times 10^{-12}\,\mathrm{F/m}$. A plot of eqs.(1)–(4) is reported in Fig.(1) for $\hbar\omega = 0.8\,\mathrm{eV}$ (corresponding to a free-space wavelength of 1550 nm) in the range of chemical potentials that will be used in the present paper. The left figure is related to the absorption coefficient of graphene and holds for both positive and negative values of the chemical potential. The right panel refers to the dielectric constant. It includes the imaginary part of the conductivity. Being the imaginary part of the conductivity an odd function of μ_C, both the cases of $\mu_C > 0$ and $\mu_C < 0$ are shown (solid and empty circles, respectively).

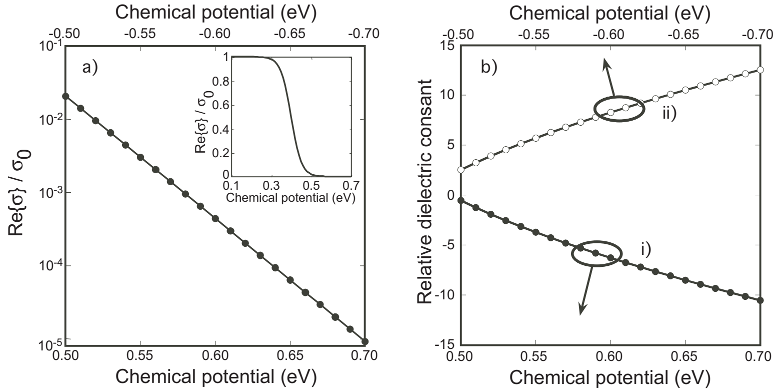

Fig. 1. a) (left panel): real part of the graphene conductivity for $\hbar\omega = 0.8$ eV (corresponding to a free-space wavelength equal to 1550 nm) vs the applied chemical potential μ_C. Inset: same quantity on a broader range of applied chemical potentials. b) (right panel): relative dielectric constant of graphene vs. the applied chemical potential (curves labeled as i) and ii) respectively refer to positive and negative values of the chemical potential).

Interestingly, in geometries including two separate layers of graphene, forming a capacitor, biasing in series the two plates induces equal in amplitude but opposite in sign values of σ_I. This condition leads to almost identical phase modulation in each layer, though with opposite sign from one the other. The overall effect is that the two phase modulations cancel each-other.

It is worth mentioning that this geometry has been used in ref.[6] where amplitude modulation was demonstrated and, for the reasons above, phase modulation did not occur.

In the present paper we show that, if properly biased, a variation of the imaginary part of graphene's conductivity may produce a visible change of the *phase* of the propagating wave. Notice that eqs.(1) and (4) show that when a bias is applied to a graphene layer, both the real and imaginary parts of its conductivity change. Thus, a modulator based on the tunability of graphene's complex conductivity will in general modulate both the phase and the amplitude of the optical wave.

In order to separate amplitude or phase modulation, different operating ranges must be used. With reference to Fig.(1), for $|\mu_C|$ between 0.3 to 0.5 eV, a large variation of the real part of graphene's conductivity is observed (see the inset in the left panel of the figure). In the same range, the imaginary part of the conductivity changes as well (see eqs. Eqs.(1) and (4)), leading to a signal that is both modulated in amplitude and phase. When using two independent layers as in ref.[6] the phase contributions arising from the two layers cancel each other. A pure amplitude modulation has to contain two layers with equal in amplitude and opposite in sign chemical potentials.

In the range $|\mu_C| > 0.5$ eV, the real part of graphene conductivity drops to negligible values: graphene has become an optically transparent material. Any change of the conductivity will now reflect on the dielectric constant only, eventually leading to phase modulation of the traveling signal. Differently from the previous case, if two independent layers of graphene are used, the same chemical potential has to be applied to the layers in order to achieve phase modulation. That is, the layers have to biased in parallel rather than in series.

3. Phase modulation in the straight-waveguide configuration

We have mentioned above that graphene's conductivity can be changed by adding (or removing) electrical charges on it. This can be done by realizing a capacitor in which one of the armatures is formed by a graphene layer. In Fig.(2) we show a possible configuration with two layers of graphene. The capacitor is between each graphene layer and the metal contact located outside the guiding region. The position of the capacitor differs from the configuration of ref.[6] because we want to avoid to charge the two layers of graphene with opposite sign charges. This difference is the most important difference with respect to the previous configuration because the real part of the conductivity, σ_I is an odd function that changes sign when changing sign of the chemical potential. In Fig.(2) we show an example of configuration in which the two layers are connected in parallel. The one layer or multiple layer configuration are similar, the electrical circuit is simply repeated.

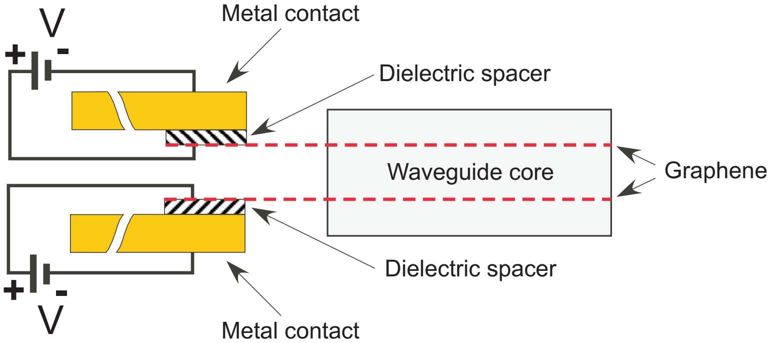

Fig. 2. Schematic diagram (not to scale) of a waveguide comprising two graphene layers biased so to obtain phase modulation.

Numerical simulations with the waveguide schematically depicted in Fig.(2) were performed. A symmetric waveguide was used, where two graphene layers (each having a thickness equal to 0.34 nm) were separated by 7 nm. Silicon enriched nitride ($Si_xN_{(1-x)}$) was the dielectric forming the high index contrast waveguide. The cladding was silica.

The dielectric constants used in simulations were equal to 4.7568 for silicon enriched nitride, and 2.25 for silica. The thickness of both the top and bottom layers was equal to 200 nm (so that the overall waveguide height was roughly equal to 400 nm), and the waveguide width was set equal to 900 nm. Propagation of the fundamental TE mode was considered at the propagating wavelength $\lambda_0 = 1550\,\text{nm}$.

For values of the chemical potential between 0.50 and 0.70 eV, we varied the real and imaginary part of the complex graphene's conductivity, and we numerically computed the complex effective index of the fundamental TE mode. Results of this analysis are reported in Fig.(3).

In the left panel of the figure we show the phase change per unit length that is observed when varying the applied chemical potential. Consider a phase modulator working in the chemical potential range spanning from 0.50 to 0.60 eV. A phase shift of $\sim -2.9\pi$ radians would be obtained in this case for each mm of waveguide. Full $-\pi$ phase shift would require a waveguide length equal to $\sim 350\,\mu$m. Observe however that the right panel of the figure shows that whenever $\mu_C = 0.50$ a non-negligible absorption is still present, due to the residual real part of the graphene's conductivity. This is in the order of 4.7 dB/mm for $\mu_C = 0.50\,\text{eV}$, dropping to 0.1 dB/mm values for $\mu_C = 0.60\,\text{eV}$. The differential absorption across 350 μm of waveguide would hence be in the order of 1.6 dB.

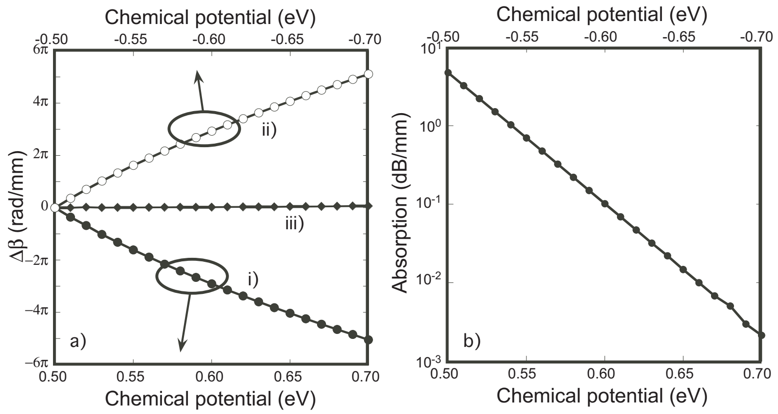

Fig. 3. a) (left panel): variation of the phase constant vs the applied chemical potential. Zero is arbitrarily chosen in correspondence to the phase displacement experienced by the wave when $\mu_C = 0.50\,\text{eV}$. b) (right panel): attenuation across a one mm long straight waveguide vs the applied chemical potential. Note the log scale in the vertical axis. Computations have been made for $\lambda = 1550\,\text{nm}$.

A better result in terms of residual amplitude modulation could be obtained by switching the chemical potential from, say, 0.60 to 0.70 eV. In this case, the waveguide length should be raised to about 470 μm in order to obtain a full $-\pi$ phase modulation, but the residual amplitude modulation would be limited to less than 0.1 dB.

As a general rule, since the absorption scales exponentially with increasing chemical potentials (notice that the right panel of Fig.(3) is in log scale), larger values of μ_C allows for reduced residual amplitude. It is important to note the increase of bias voltage is limited by the breakdown of the dielectric spacer in the contact region of graphene. In fact Hanson has shown that, at least for an isolated sheet of graphene, the following relation holds between the chemical potential and the carrier density [10]

$$n_s = \frac{2}{\pi\hbar^2 v_F^2} \int_0^{+\infty} \varepsilon \left[f_d(\varepsilon) - f_d(\varepsilon + 2\mu_C) \right] d\varepsilon \simeq \frac{(e\mu_C)^2}{\pi\hbar^2 v_F^2} \quad , \tag{5}$$

where $f_d(\varepsilon) = \left(e^{(\varepsilon-\mu_C)/k_BT}+1\right)^{-1}$ is the Fermi–Dirac distribution, $v_F \simeq 9.5\times 10^5$ m/s the Fermi velocity and e the electron charge.

Such density should be deposited on the armatures of the capacitor schematically depicted in Fig.(2). Let us denote as S the capacitor surface, and assume that its dielectric spacer is constituted by a $d = 7$ nm thick alumina layer with relative dielectric constant $\varepsilon_{\mathrm{Al_2O_3}} \simeq 10$. The driving voltage needed to charge the capacitor is

$$V = \mu_C + \frac{Q}{C} = \mu_C + \frac{e n_S S}{\varepsilon_0 \varepsilon_{\mathrm{Al_2O_3}} S/d} = \mu_C + \frac{e d\,(e\mu_C)^2}{\varepsilon_0 \varepsilon_{\mathrm{Al_2O_3}} \pi \hbar^2 v_F^2} \quad .$$

One finds $V = \{3.1, 4.3, 5.8\}$ Volt for $\mu_C = \{0.5, 0.6, 0.7\}$ eV, respectively. For instance, in the range of chemical potentials from 0.5 to 0.6 eV the electro–optical efficiency is 2.4π/mm/V ($V_\pi L_\pi \simeq 0.04$ V cm).

Observe finally that the voltage required to drive graphene at 0.7 eV is possibly not yet large enough to cause break-down of the alumina within the capacitor armatures, but much greater values than $\mu_C = 0.7$ eV can hardly be realized in practice.

4. Phase modulation in the ring configuration

The straight waveguide configuration has the advantage of being inherently wideband. On the downside, phase modulation in straight waveguides requires rather long propagation. We aim at showing now that full phase modulation can be obtained in a much more compact device if a ring configuration is considered instead. Clearly microring resonances imply reduction of bandwidth. However, we show in the following that operations over bands in the order of hundreds of GHz can still be obtained, with footprint dimensions limited to hundreds of square microns.

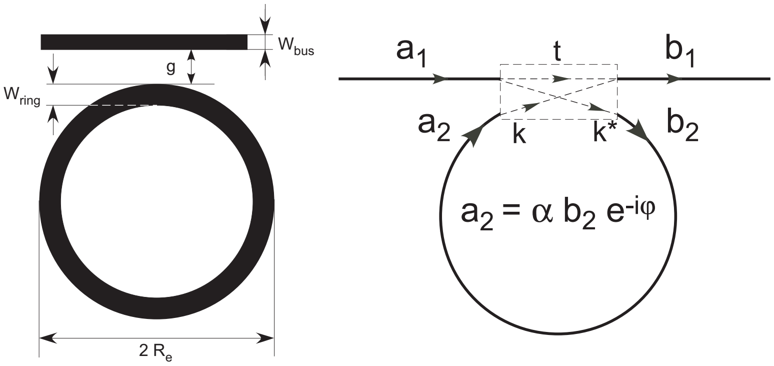

Fig. 4. Left panel: Schematic diagram of the ring configurations phase modulator. Right panel: fields in the ring structure, with definition of the straight waveguide and ring single pass transmission, t and α, respectively.

In Fig.(4) we show a schematic diagram of the all–pass microring filter we use as an example to show the effect of the change of graphene conductivity in the filter phase shift. The filter contains a straight bus waveguide made of silicon enriched nitride with width $W_{\mathrm{bus}} = 700$ nm and height $H_{\mathrm{bus}} = 400$ nm which is coupled to a microring. The microring waveguide contains two layers of graphene and its width is $W_{\mathrm{ring}} = 900$ nm. Bus to ring gaps where chosen in the range $g \simeq 100 \div 200$ nm, and the microring radius $R_{\mathrm{e}} \simeq 9 \div 15\,\mu$m, respectively.

The right panel of the figure shows the fields in the ring and in the bus. The input-to-output transfer function reads [11]

$$\frac{b_1}{a_1} = \frac{t - \alpha e^{-i\varphi}}{1 - \alpha t e^{-i\varphi}} \quad . \tag{6}$$

We remark that in this equation α is the amplitude transmission of the field through a single ring round-trip, while t is the bus-to-bus (or ring-to-ring) coupler transmission, respectively. Moreover, φ is the field phase shift in a single ring round-trip. Let us now denote as T and ψ the amplitude and phase transfer function of the ring structure, respectively. They read

$$T = \left|\frac{b_1}{a_1}\right|^2 = \frac{(\alpha - |t|)^2}{(1 - \alpha|t|)^2} \quad , \tag{7}$$

$$\psi = \text{phase}\left(\frac{b_1}{a_1}\right) = \arctan\left(\frac{\alpha(1-t^2)\sin\varphi}{t(1+\alpha^2) - \alpha(1+t^2)\cos\varphi}\right) \quad . \tag{8}$$

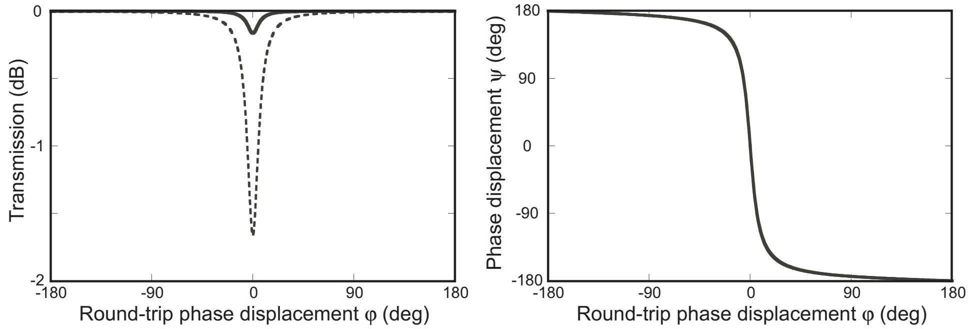

Fig. 5. Left panel: overall bus-to-bus transmission for coupler transmission $t = 0.9$, and ring transmission $\alpha = 0.99$ (dashed line) or $\alpha = 0.999$ (solid line). The abscissa is the round–trip phase shift φ. Right panel: overall bus-to-bus phase shift. Dashed and solid lines still refer to $\alpha = 0.99$ and $\alpha = 0.999$ and coincide.

A plot of eq.(7) and (8) is reported in the left and right panels of Fig.(5), respectively. Coupler transmission $t = 0.9$ was used (i.e. power coupling coefficient of 18.5%), along with $\alpha = 0.99$ (dashed line) and $\alpha = 0.999$ (solid line). These values would correspond to a ring loss equal to 1.2 dB/mm and 0.1 dB/mm respectively when the ring radius is equal to 12 μm. The large coupling in the example is to show the efficiency of the resonant phase shift even for designs highly tolerant to fabrication errors on the centering of the resonant wavelength. Lower values of coupling coefficient would enhance the graphene induced phase shift but would be more critical because of the need of the trimming of the resonant frequency of the microring.

Dashed and solid lines are also used in the right panel of the figure, but they almost coincide. If we had further increased the ring transmission $\alpha \to 1$, the amplitude transfer function T would have been flat (i.e. the ring would have behaved as ideal all-pass filter), while the phase curve would have remained unchanged. In a real device the combination of a low loss ring waveguide and the low loss propagation with a graphene biased in the region of negligible loss leads to an almost ideal all pass filter, i.e. a device with small insertion loss and large externally induced phase change. This differs from other phase modulation effects achievable in photonic integrated circuits in which phase modulation is always at expenses of a large insertion loss caused by a non-negligible contribution of induced absorption, see for instance plasma dispersion effect, Franz Keldish or even Quantum Confined Stark effect.

Thus, phase modulation can be achieved by varying only the refractive index of the waveguide in the ring. This leads to filter frequency tuning that can be exploited for tuning/trimming, switching or modulation. In all these respects, we believe that graphene may offer unique opportunities. As a matter of fact, we have seen above that there is a wide range of chemical potentials which give rise to really small absorptions: the right panel of Fig.(3) shows that absorption is lower than 0.1 dB/mm for chemical potentials above $\mu_C = 0.58\,\mathrm{eV}$. It would drop even further for $\mu_C > 0.7\,\mathrm{eV}$, but the break-down voltage of the dielectric in the capacitor limits too large bias voltages. At the same time, graphene's relative dielectric constant varies by a factor of 2 over the $0.58 < |\mu_C| < 0.70\,\mathrm{eV}$ range.

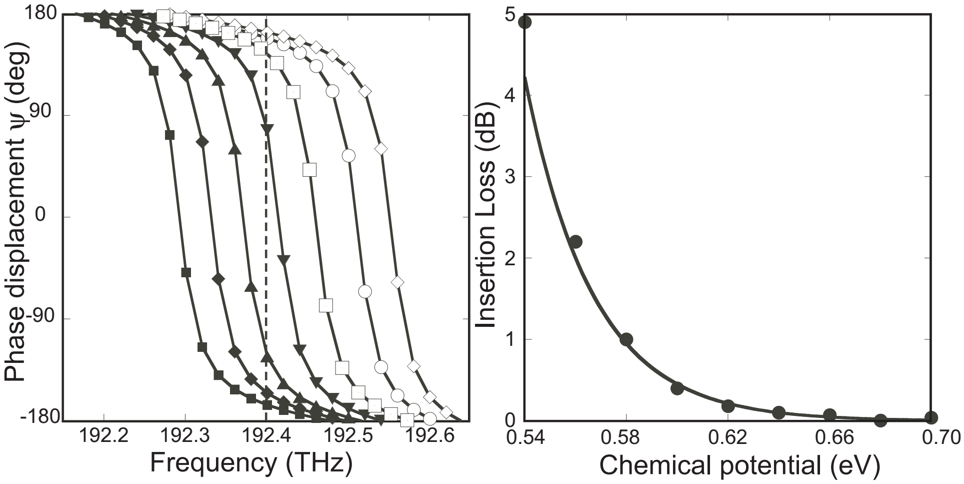

Fig. 6. Left panel: phase displacement ψ vs. frequency for chemical potential $\mu_C = 0.58\,\mathrm{eV}$ (filled squares), $\mu_C = 0.60\,\mathrm{eV}$ (filled diamonds), $\mu_C = 0.62\,\mathrm{eV}$ (filled up-triangles), $\mu_C = 0.64\,\mathrm{eV}$ (filled down-triangles), $\mu_C = 0.66\,\mathrm{eV}$ (empty squares), $\mu_C = 0.68\,\mathrm{eV}$ (empty circles) and $\mu_C = 0.70\,\mathrm{eV}$ (empty diamonds), respectively. Right panel: insertion losses vs. the applied chemical potential.

Fig.(6) shows the behavior of the ring as a phase modulator. In the left panel, the phase shift ψ vs. frequency is shown for chemical potential $\mu_C = 0.58\,\mathrm{eV}$ (filled squares), $\mu_C = 0.60\,\mathrm{eV}$ (filled diamonds), $\mu_C = 0.62\,\mathrm{eV}$ (filled up-triangles), $\mu_C = 0.64\,\mathrm{eV}$ (filled down-triangles), $\mu_C = 0.66\,\mathrm{eV}$ (empty squares), $\mu_C = 0.68\,\mathrm{eV}$ (empty circles) and $\mu_C = 0.70\,\mathrm{eV}$ (empty diamonds), respectively. In the right panel, insertion losses vs. the applied chemical potential are shown. A few comments are in order: phase curves are in close agreement with theoretical ones (see eq.(8) and Fig.5). Wide phase modulation can be achieved upon application of a relatively modest change the chemical potential. At any given frequency, full 180 phase shift requires a variation of the chemical potential in the order of 0.02 eV. For instance, the vertical dashed line in the left panel of the figure shows the phase shift for frequency equal to 194.2 THz. The phase is lower than -90 degrees when $\mu_C = 0.62\,\mathrm{eV}$ (filled up-triangles). Whereas, it is roughly equal to +90 degrees for $\mu_C = 0.64\,\mathrm{eV}$ (filled down-triangles)

Losses are lower than 0.5 dB for any chemical potential larger than 0.6 eV. In addition, a change of the chemical potential in the order of 0.02 eV causes a really minor variation of losses. That is, almost pure phase modulation without residual amplitude modulation can be achieved. Both in terms of losses and of achievable phase shift, the operating point of the device can be anywhere in the range $\mu_C > 0.6\,\mathrm{eV}$. This suggests that the device could be operated as follows: a bias to set the operation frequency, and full phase shift could be obtained by modulating the applied voltage around the bias. This way, trimming the resonant frequency with no heating can be achieved and the complete functionality can be operated with negligible power consumption.

Finally, observe that the bandwidth of operation solely depends on the applied voltage to induce the modification of the graphene's dielectric constant. Thanks to the efficiency of the effect it is not necessary to resort to large cavity Q to enhance the effect. The choice of the cavity Q would only impact on the steepness of the phase transition across the resonant frequency.

5. Conclusions

In conclusion we have shown that single or double layers of graphene embedded in the core of a waveguide can be exploited to induce a change in the waveguide effective index. The index change occurs when a suitable bias induces carriers in the graphene conduction band with the condition that $|\mu_C| > \hbar\omega/2$. Under this regime graphene results transparent and a tuning of the bias voltage (i.e. a change of the carrier concentration in the graphene layer) provides a large change in the real part of the dielectric constant. Phase modulation of TE modes in straight waveguides and in microring resonators have been shown. Applications to several optoelectronic functionalities as modulators, tunable filters, switches, etc., could benefit either from the efficiency of the effect and for the negligible value of insertion loss achievable. In addition the surface charge induced in graphene is obtained by charging a capacitor, as a consequence the induced changes do not require current flow with benefits in terms of power consumption.

Acknowledgements

This work was supported by TIIF (Innovative Technologies for Photonic Integration) Project. P.G. is consultant at University of Udine.